Giant magneto-optical Faraday effect of graphene on Co in the soft x-ray range

H.-Ch. Mertins,[1,*] C. Jansing,[1] M. Krivenkov,[2] A. Varykhalov,[2] O. Rader,[2] H. Wahab,[3] H. Timmers,[3] A. Gaupp,[2] A. Sokolov,[2] M. Tesch,[2] and P. M. Oppeneer[4]

[1]*University of Applied Sciences Münster, Stegerwaldstrasse 39, D-48565 Steinfurt, Germany*
[2]*HZB, Albert-Einstein-Strasse 15, D-12489 Berlin, Germany*
[3]*University of New South Wales, Canberra, ACT 2600, Australia*
[4]*Department of Physics and Astronomy, Uppsala University, Box 516, S-751 20 Uppsala, Sweden*

Using polarization analysis of linearly polarized synchrotron radiation we demonstrate the existence of a giant magneto-optical Faraday effect at the carbon $1s$ edge of single-layer graphene on Co, reaching Faraday rotation angles of 2.9×10^5 deg/mm. This value is of the order of those observed at the Co $3p$ and $2p$ edges. Using element-selective magnetic hysteresis curves we find that graphene on Co exhibits ferromagnetic order. The magnetism in graphene is found to be carried by and be strongly enhanced by aligned π orbitals of carbon atoms. It is induced by hybridization with the Co $3d_z2$ orbitals while carbon σ bonds show negligible magnetism due to insignificant hybridization with Co. From additional x-ray magnetic circular dichroism and transversal magneto-optical Kerr effect spectra a magnetic moment of $0.14 \mu_B$ is estimated for graphene. From Faraday spectra the complete set of x-ray magneto-optical constants of graphene has been deduced which allows for future modeling of magneto-optical devices based on graphene. The strong magnetism in graphene results from hybridization of carbon p_z and metal $3d$ orbitals. Atoms of the graphene sublattice A, placed on top of Co, lead to strongest hybridization with Co $3d_z{}^2$ orbitals. Carbon atoms of sublattice B, and those of rotated graphene domains without Co atoms beneath, hybridize with each other and with $3d_{xz}$ and $3d_{yz}$ orbitals of neighboring Co atoms forming tilted p_z bonds. We show that the related reduction of A-B symmetry leads to a splitting of the spin-polarized density of conduction-band states which is responsible for the strong magneto-optical Faraday effect.

I. INTRODUCTION

Graphene, a one-atom-thick carbon layer, exhibits remarkable transport properties that could facilitate new technical applications [1,2]. The negligible spin-orbit coupling in graphene enables ideal spin transport properties that may open up new avenues for applications of graphene in spintronics [2,3]. Several different techniques are being discussed to fabricate magnetic graphene: creating vacancies by proton irradiation [4], doping with hydrogen [5,6], and deposition of nonmagnetic molecules [7]. However, these techniques do not allow for standardized industrial production and applications at room temperature. Contacting graphene to metallic, ferromagnetic substrates seems promising for applications [3,8]. However, the understanding of essential chemophysical processes as hybridization of the $3d$ orbitals of metallic substrates with those of carbon, the related induction of magnetic moments in graphene, as well as their alignment is still missing. Only for graphene on Ni do experimental x-ray magnetic circular dichroism (XMCD) data exist [8] which give a rough estimation of the magnetic moment of carbon atoms induced by Ni to be in the range 0.05–0.1 μ_B. Recent photoelectron investigations reveal magnetism of graphene on Co and Ni detected by the spin polarization of occupied valance-band states focusing on the small region around the Dirac point [3,9,10], but appropriate knowledge about the unoccupied conduction-band (CB) states, hybridization with metal $3d$ states, and resulting magnetism is missing. Magneto-optical investigations of graphene on SiC substrates have been conducted with terahertz radiation showing Faraday rotation in large magnetic fields of up to 8 T [11]. Here, inter-Landau-level transitions of CB electrons are excited at cyclotron resonance energies in the range of some meV. While these experiments are suited to reveal transport properties [1,11] of graphene on transparent SiC they are not able to characterize the magnetic state of graphene since monitoring of hysteresis curves is impossible. Moreover, these experiments do not allow for investigations of graphene on metallic substrates due to the absorption of terahertz radiation in metals.

The magnetic state of individual elements in a material can be selectively probed with soft x-ray magneto-optical spectroscopies exploiting polarized synchrotron radiation [12]. In particular the XMCD serves as a powerful tool for the quantitative determination of both the magnetic orbital and the spin moment exploiting sum rules for resonant excitations from $2p$ to $3d$ states in $3d$ transition metals [12], but in principle this method is not applicable to graphene since appropriate sum rules do not exist for excitations from $1s$ to $2sp^2$ states in carbon. Also, XMCD spectroscopy cannot detect orbital bond directions.

*Corresponding author: mertins@fh-muenster.de

In this paper we show that these drawbacks can be overcome by exploiting linearly instead of circularly polarized light, namely, applying Faraday spectroscopy bearing great advantages [13–15] as the element selective and direction sensitive determination of hybridization of the metallic substrates' $3d$ orbitals with the graphene π and σ bonds.

II. THEORY AND EXPERIMENTAL SETUP

A. Methodology

The Faraday effect describes the rotation of the polarization plane of linearly polarized light, when transmitting a sample that has a magnetic moment parallel or antiparallel to the light's direction. In addition the state of the polarization changes to elliptical [14,16]. The experimentally employed geometry to detect the x-ray Faraday effect of graphene is shown in Fig. 1.

To describe the Faraday effect quantitatively the incident linearly polarized light beam is decomposed into two circularly polarized waves of opposite helicity. The interaction of these two waves with the magnetic material is described by its complex optical constants $n_\pm$ (+ and − refer to the orientation of photon spin aligned parallel or antiparallel to the magnetic moments of the sample). The optical constant can be written as

$$n_\pm = 1 - (\delta_0 \pm \Delta\delta) + i\,(\beta_0 \pm \Delta\beta) \tag{1}$$

with δ_0 the real dispersive part and β_0 the absorptive imaginary part for linearly polarized light, respectively. The circular dichroism is expressed by $\Delta n = n_+ - n_- = -\Delta\delta + i\Delta\beta$. Upon transmission of a film with thickness d a phase change $\Delta\delta$ between the left- and right-handed polarized waves appears which leads to a rotation of the polarization pane. In addition, the dichroism $\Delta\beta$ in the absorption leads to a transmitted beam with elliptical polarization. The complex Faraday equation can be written as [16]

$$\varphi + i \, \tan\varepsilon \approx \frac{d\,\pi}{\lambda}\, i\, \frac{\varepsilon_{xy}}{\varepsilon_{xx}^{1/2}} \tag{2}$$

with wavelength λ. The off-diagonal permittivity ε_{xy} is the magneto-optically active component, which is antisymmetric in the magnetization. For a linearly polarized wave both the ellipticity ε and the rotation angle φ of the transmitted light are related directly to the optical constants as described in first-order approximation by the following equations [16]:

$$\varphi = \frac{2\,\pi}{\lambda} d\,\Delta\delta \,/ \tan\theta, \tag{3a}$$

$$\tan 2\varepsilon = 2\frac{2\,\pi}{\lambda} d\,\Delta\beta \,/ \tan\theta \approx A_C. \tag{3b}$$

The angle θ of the incident light, measured to the sample surface, enters the equation via the effective sample thickness $d/\sin\theta$ and via the angle dependent interaction of circularly polarized light with the magnetic field B which scales with $B\cos\theta$. Alternatively, the magneto-optical constant $\Delta\beta$ can be measured with circularly polarized light in XMCD reflection experiments. It is deduced from the asymmetry parameter A_C, defined as $A_C = (T_+ - T_-)/(T_+ + T_-)$. The transmission coefficients of circularly polarized x rays with magnetic field oriented parallel or antiparallel to the light's direction are given by $T_\pm = \exp\{-4\,\pi\,d\,(\beta_0 \pm \Delta\beta)/\lambda\}$. For small ε the relation $A_C \approx \tan 2\varepsilon$ holds [14,16]. Note that XMCD intensity experiments yield only the imaginary part $\Delta\beta$ of the optical constant while the Faraday polarization experiment yields the complete set of magneto-optical constants.

For discussion of the interaction of the light at the graphene-metal interface (Fig. 1) we have to consider two reflected rays. One part of the incident intensity I_0 is directly reflected at the graphene surface and a second part, which has transmitted the graphene layer, is reflected at the substrate and passes the graphene layer again. Upon reflection two different strong phase shifts ϕ_1, ϕ_2 appear at the graphene surface and at the metallic substrate, respectively. For the case of a difference $\alpha = \phi_1 - \phi_2$ between these phase shifts interference has to be taken into account. An additional phase shift due to the optical path length is negligible for the extremely thin graphene layer. Thus the intensity I after interaction with the sample is described by

$$I/I_0 = R_G + T_G^2 R_M + 2\,|r_G r_M| T_G \cos\alpha, \tag{4}$$

with the reflectance $|r_G|^2 = R_G$ and the transmittance of graphene T_G $(T_G = |t_{GV}|^2 = |t_{VG}|^2$, with the transmission coefficients from vacuum to graphene), and $|r_M|^2 = R_M$ being the reflectance of the substrate acting as mirror. Reflection of soft x-ray light on the inside of the graphene layer is insignificant and can be neglected. First-order approximations show that the transmission through the graphene dominates over the reflectance at the graphene top surface since $r_M \approx 5\,r_G$. This value was obtained from independent reflection experiments of graphene [17] and was confirmed by model calculations using the computer code REFLEC [18] and optical constants from the Henke table [19].

B. Experimental setup

The room-temperature experiments were performed on the undulator beamline UE56-2-PGM2 of BESSY [20] using the BESSY ultrahigh-vacuum polarimeter chamber [13]. The spectral resolution near 290 eV was set to $E/\Delta E = 2000$ with energy calibration better than 0.1 eV. The electric-field vector E of the linearly polarized incoming light could be set alternatively parallel to the π^* orbitals (E_p in Fig. 1, p geometry) or perpendicular to the π^* orbitals (E_s, s geometry)
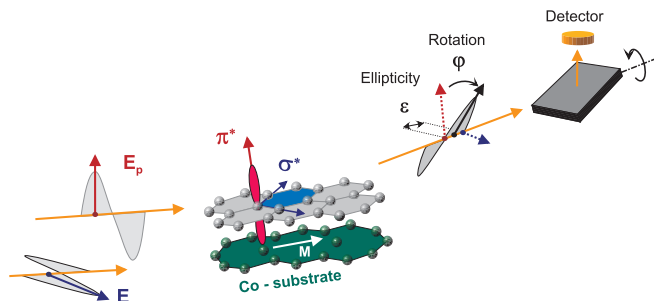

FIG. 1. Setup for the detection of the x-ray Faraday effect, i.e., the rotation φ and ellipticity ε of linearly polarized light after its interaction with graphene on Co using polarization analysis. The directions of the π^* and σ^* bonds of graphene and the orientations of electric field E_p and E_s for p- and s-polarized light are indicated.
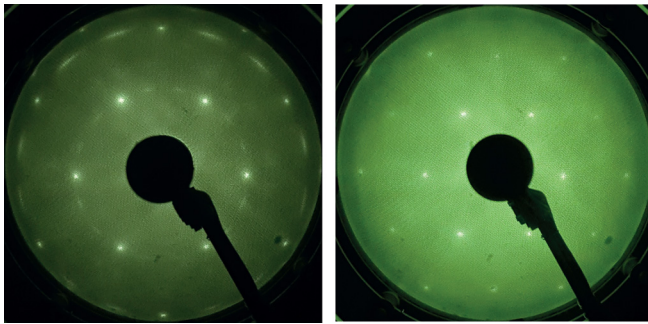
FIG. 2. (a, b) LEED pattern of graphene/Co (0001)/W for 285 eV (a, left panel) and 185 eV (b, right panel), showing arcs which indicate a rotation of a part of graphene flakes which are not aligned with the substrate.

with fixed angle of incidence $\theta = 20° \pm 0.3°$, measured to the surface. The polarization state of both the incident and reflected light was monitored by rotating a Cr/Sc reflection multilayer and monitoring the intensity [17] (Fig. 1). The degree of linear polarization of incident light ($P_L > 0.99$) was measured independently. The evaluation procedure of the polarization data is described in Ref. [14]. For XMCD reflection spectroscopy the undulator was running in a newly developed mode of optimized gap-shift coupling to provide a high degree of circular polarization S_3 with $0.77 < S_3 < 1$ at the σ resonance and $0.4 < S_3 < 1$ across the π resonance which has been measured independently according to a procedure described in Ref. [13].

In situ exchange and removal of samples enabled a quasisimultaneous polarization analysis of the incident and reflected beam as well as measurements of the incoming light for the determination of the absolute reflectance. All recorded reflection spectra were corrected for contributions from higher-order light applying a procedure described in Ref. [21]. The higher-order light originates at the monochromator and cannot be avoided and the correction is necessary. Polarization measurements are, however, not significantly affected by higher-order light, since the Cr/Sc multilayer polarization analyzer suppresses second-order light by a factor of 100 and third-order light by a factor of 50, respectively.

The samples were monolayer graphene deposited on 5.8-nm hcp Co (0001) grown on W(110) substrate characterized prior to measurement by scanning tunneling microscopy (STM) and low-energy electron diffraction (LEED) [3]. The LEED pattern is shown in Figs. 2(a) and 2(b) indicating a slight misorientation of graphene relative to the Co lattice. Any in-plane magnetization geometry could be set by *in situ* rotation of permanent magnets with maximum field strength of 250 mT [22]. Hysteresis curves were achieved by applying a solenoid creating in-plane fields of up to +/− 50 mT.

III. RESULTS

A. Reflectance

The reflectance R_s of the pure substrate Co/W without graphene calculated with REFLEC using the optical constants from the Henke table [18,19] is plotted in Fig. 3(a), dotted line. Across the carbon 1s edge it does not show carbon related struc-
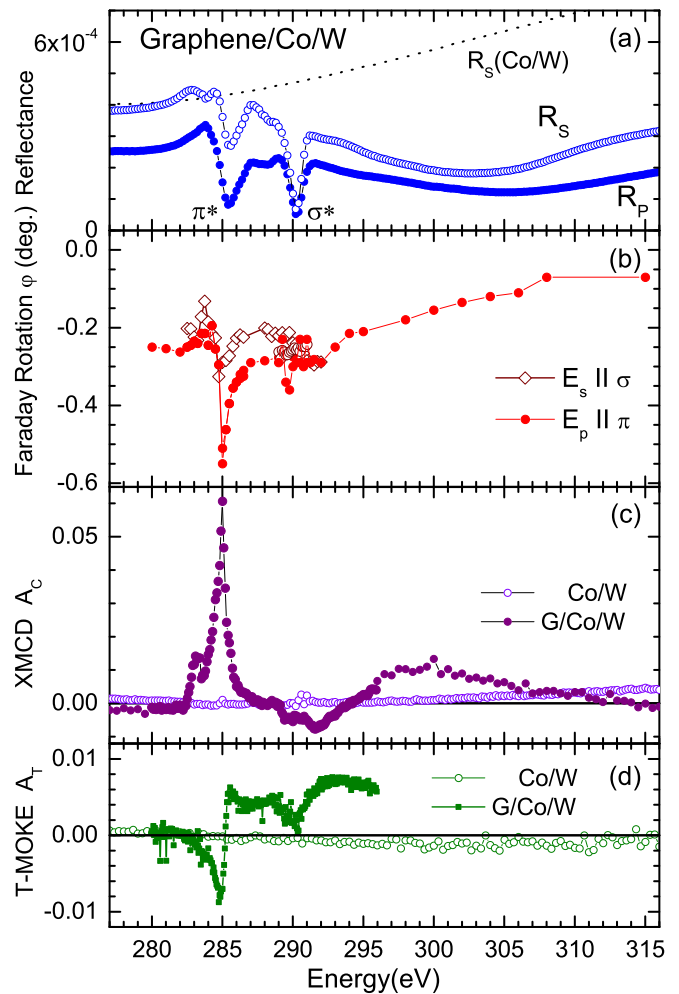

FIG. 3. Magneto-optical spectra measured on graphene/Co/W each with $\theta = 20°$ angle of grazing incidence. (a) Absolute reflectances R_p and R_s obtained with orientation of electric field E_p parallel to $\pi*$ bonds and E_s parallel to $\sigma*$ bonds, respectively. Calculated R_s for the substrate Co/W (dotted line). (b) X-ray Faraday rotation spectrum measured for *p*-polarized light (filled symbols) and *s*-polarized light (open symbols) on in-plane magnetized graphene. (c) XMCD A_C obtained with circularly polarized light (filled symbols for G/Co/W). The reference substrate without graphene does not show magnetic signals (open symbols). (d) T-MOKE asymmetry A_T measured with *p*-polarized light (filled symbols for graphene/Co/W) and open symbols for reference sample Co/W.

tures. For graphene on Co/W the absolute reflectances R_s and R_p for *s*- and *p*-polarized light, respectively, show dominant structures at the $\pi*$- and $\sigma*$-resonance energies [Fig. 3(a), open and filled circles]. Below the $\pi*$ edge the signal is dominated by the reflectance of the Co/W substrate [Fig. 3(a), dotted line]. With increasing energy towards the $\pi*$ resonance the intensity increases slightly due to increasing reflection at the graphene surface before the absorption in the graphene layer increases leading to a reduction of the transmittance T_G [second term of Eq. (4)] through the graphene layer resulting in a minimum at 285.4 eV. In addition, rays reflected from the graphene top layer and the graphene-substrate interface lead to destructive interference [third term in Eq. (4)] resulting

in a further decrease of the signal. These effects have been discussed quantitatively in detail for graphene on Cu [23]. Both processes clearly show that the transmittance dominates over reflection at the graphene surface and that we have to treat our observations as x-ray Faraday effect which occurs upon transmission of the graphene layer. The magneto-optical Kerr effect which occurs upon reflection solely at the graphene layer may contribute too, but less than 20% according to the small reflectance R_G at the graphene surface as deduced from calculations using REFLEC [18,19]. While *p*-polarized light shows stronger dips at the $\pi*$ excitation, *s*-polarized light shows stronger dips at the $\sigma*$ excitations (290.2 eV) since then the electric-field vector is parallel to the in-plane oriented σ bonds (Fig. 1).

B. Faraday effect

The x-ray Faraday rotation spectrum [Fig. 3(b)] was measured at fixed photon energies across the C 1*s* edge while the in-plane magnetization components $\pm B\cos\theta$ were switched parallel or antiparallel to the light's direction. Faraday rotation values of $\varphi = 0.2°$ occur over a broad energy range across the C 1*s* edge. Additionally, resonantly enhanced peak values of $\varphi = 0.55°$ occur at 285.0 eV for *p*-polarized light due to the interaction with $\pi*$ orbitals. A further slightly enhanced Faraday rotation is observed at 290.0 eV due to excitation into upper $\pi*$ states at the Γ point of the Brillouin zone. To test the specific roles of $\pi*$ and $\sigma*$ orbitals for magnetism in graphene we measured the Faraday rotation for incident *s*-polarized light (Fig. 1). For *s* polarization the Faraday rotation is expected to disappear at the $\pi*$-resonance energy near 285 eV since at this energy no contribution of $\sigma*$ orbitals to the density of states (DOS) exists. Our experiments show a reduction of the Faraday rotation but the expected complete disappearance is not observed [Fig. 3(b), open symbols]. A relatively large resonantly enhanced Faraday rotation of 0.32° remains. This observation demonstrates that tilted $\pi*$ orbitals must exist which show a component parallel to the electric field of the incident *s*-polarized light. We shall explain this tilt by different hybridization of the carbon $\pi*$ and Co 3*d* orbitals below. A second observation for *s*-polarized light is the lack of resonantly enhanced Faraday rotation values at the $\sigma*$ resonance near 290 eV (Fig. 3(b), open symbols). This unambiguously shows that, despite the parallel alignment of the electric field with the $\sigma*$ orbitals and the strong contribution of the DOS at this energy, $\sigma*$ orbitals do not contribute to the magnetism in graphene.

Note that our observation is indeed the magneto-optical Faraday effect since it appears solely upon switching the magnetization direction. This Faraday effect is obviously distinct from the nonmagnetic natural birefringence or natural linear dichroism which is related to the two-dimensional structure of nonmagnetic graphene as reported in detail in Ref. [17]. To detect the natural linear dichroism a specifically experimental geometry distinct from that shown in Fig. 1 is required [17]. Furthermore, for our experimental Faraday geometry (Fig. 1) the nonmagnetic natural dichroic effects must disappear [17]. As a second proof the pure Co/W substrate without graphene was investigated, but no magnetic signal could be detected,

either as Faraday effect or as XMCD signal [see discussion below and Figs. 3(c) and 3(d)].

Generally the Faraday rotation scales with the thickness d of the transmitted sample and the projection $\cos\theta$ of the light's direction on the magnetization M according to $\varphi_F = k\,d\,M\,/\tan\theta$ where k is the Verdet constant [14,16]. Although this formula is used for thicker samples, we apply it to our extremely thin monolayer graphene with $d = 2 \times 0.34$ nm, where d is the projection of the entire path length onto the surface normal, to deduce the Verdet constant $k = (2.9 \pm 0.2) \times 10^5$ deg /mm for saturated magnetization $M = 1$. Astonishingly, this leads to a giant k value which is in the order of polycrystalline Fe or Co films of 50-nm thickness at the 2*p* and 3*p* edges and a factor of 10 larger than that in the visible range [14]. We are aware that the Verdet constant is defined to describe magneto-optical effects of thin volume samples. Since graphene must be treated as a two-dimensional system with a fixed thickness the Verdet constant may lose its originally meaning.

This giant Faraday effect of graphene peaking at the $\pi*$-resonance energy can be explained by the strong hybridization of the metal 3*d* orbitals with the $\pi*$ orbitals and their collective alignment parallel to the electric field of the incident *p*-polarized light as discussed in detail below. The element selective excitation at the C 1*s* edge proves that the observed rotation definitely originates from the carbon atoms and is not caused by excitations of the Co substrate since the Co 2*p* edge (776 eV) and 3*p* edge (68 eV) are far away.

C. Transversal magneto-optical Kerr effect, XMCD, and band structure

The magnetization of graphene was also probed employing the x-ray transversal magneto-optical Kerr effect (T-MOKE) and XMCD. Both XMCD spectra [Fig. 3(c), filled symbols] as well as T-MOKE [Fig. 3(d), filled symbols] deliver clear magnetic signals related to graphene. The XMCD asymmetry parameter $A_C = (I_+ - I_-)/(I_+ + I_-)$ is calculated by the normalized difference of intensities $I_{+/-}$ of circularly polarized x rays after transmission of the graphene layer and reflection at the Co substrate with magnetic field oriented parallel or antiparallel to the direction of circularly polarized light [12,14]. Since the asymmetry parameter A_C scales linearly with the degree of circular polarization S_3 [24] the plotted values have been normalized to S_3 which was measured independently by the BESSY polarimeter according to a procedure described in Ref. [13]. The XMCD asymmetry parameter A_C is related to the imaginary part of the Faraday effect according to Eq. (3b) providing the absorption constant which typically is measured in transmission of thin films or in electron yield absorption measurements. Large XMCD peak values of $A_C = 0.06$ are observed near 285 eV which are a factor of 6 larger than peak signals in the T-MOKE spectra [Figs. 3(c) and 3(d)].

In contrast to XMCD, T-MOKE is observed in reflection. T-MOKE spectra result from the normalized difference signal of reflected linearly *p*-polarized light which is monitored for transversal in-plane magnetization with two antiparallel directions perpendicular to the light's scattering plane. The predominance of XMCD signals over T-MOKE signals indicates that the observed magneto-optical effect is dominated

by a strong transmission process of light through graphene instead of a reflection process at the graphene top surface. This observation supports our interpretation of the observed magneto-optical effect as the Faraday effect instead of a Kerr effect.

Furthermore, XMCD spectra of an identical Co/W reference substrate without graphene do not show any magnetic signal, either in XMCD [Fig. 3(c), open symbols] or in T-MOKE spectra [Fig. 3(d), open symbols]. This proves that the observed magnetism across the C 1s edge is related to graphene. These reference samples have been exposed to air for 20 min and covered by carbon and carbenous adsorbats. However, no induced magnetism across the C 1s edge due to carbonized Co could be detected, showing that the reported magnetism is indeed related to ordered graphene.

The strong resonance of the XMCD signal at the $\pi*$ edge indicates that the magnetism in graphene is strongly related to the $\pi*$ states. Small contributions at and above the $\sigma*$ resonance are assigned to higher $\pi*$ states. In general a XMCD signal is obtained due to the spin-orbit coupling of the involved core-level states, a condition which is well fulfilled for $2p$-$3d$ excitations in $3d$ transition metals [12]. The C 1s initial states, however, show only an exchange splitting, but no spin-orbit splitting exists for s states. The required magnetic moment of the C $2p$ states is induced by the hybridization with the Co $3d$ orbitals. This leads to the observed difference in the spin-polarized DOS which is proportional to the measured XMCD spectrum. We attribute the strong features to the hybridization of the lower $\pi*$ bands and transition-metal $3d$ CB between the M and K point of the Brillouin zone. This interpretation is supported by calculations [3,9] showing the well-known [12] localization of transition-metal $3d$ states at the bottom of the CB with a strong hybridization with $\pi*$ bands over a wide range of the Brillouin zone leading to peaks in the spin-split DOS resulting from A-B symmetry breaking [3,9] as discussed below. For higher CBs, i.e., at excitation energies into $\sigma*$ states near 290 eV, transition-metal $3d$ states are negligible, which explains the weak magnetic effects at these energies.

XMCD experiments can be performed alternatively by electron yield absorption techniques. This was done for graphene on Ni [8] and graphene on Ir intercalated by Co [25,26]. Both samples show a predominant peak at the $\pi*$ resonance and negligible structures at the $\sigma*$ region. Weser *et al.* [8] obtain a peak value $A_C = 0.013$ for G/Ni. This is a factor of 4.6 smaller than our value found for G/Co which is qualitatively in agreement with the smaller magnetic moment of Ni compared to that of Co. Vita *et al.* [25,26] show the non-normalized difference spectrum for opposite magnetization from which an asymmetry parameter $A_C = 0.05$ can be estimated, which is close to our findings.

D. Magnetic moment

The magnetic moment of carbon atoms in graphene was deduced by comparing the strength of XMCD data at the C 1s edge of graphene [$A_C(C) = 0.06$] with our independent XMCD measurements at the Co $2p_{3/2}$ edge. The corresponding reflection spectra of G/Co/W for circularly polarized light with two opposite magnetization directions $M(+)$ and $M(-)$ are plotted in Fig. 4, top panel. The deduced XMCD spectrum
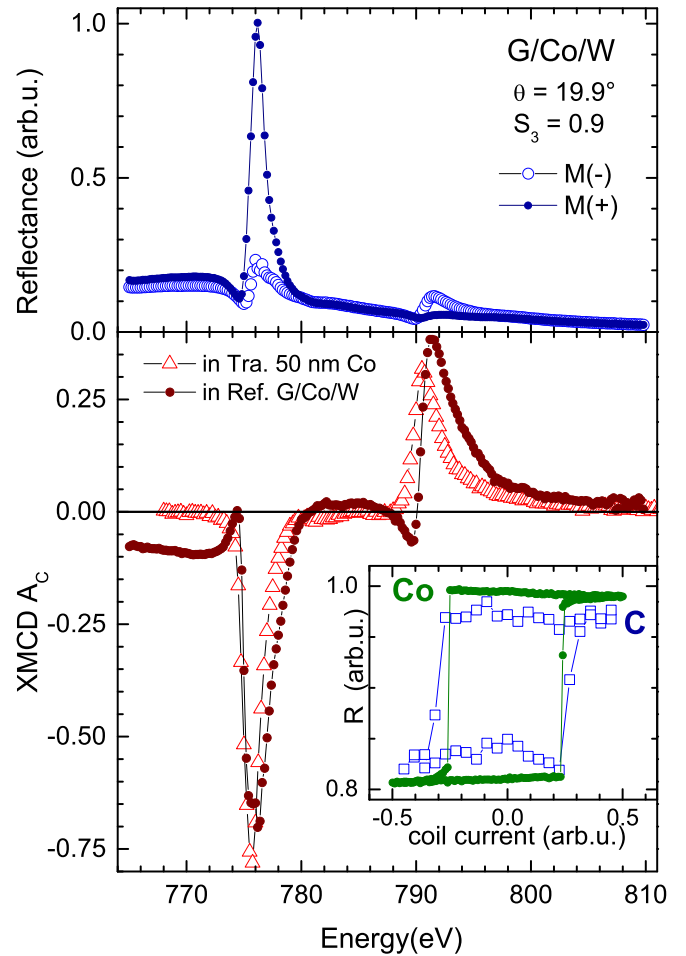

FIG. 4. Top: Reflectance spectrum across the Co $2p$ edge of graphene/Co/W with circularly polarized light ($S_3 = 0.9$) for two opposite magnetization directions with respect to the light's direction, parallel $M(+)$ and antiparallel $M(-)$, respectively, for grazing incidence angle 19.9°. Bottom: XMCD asymmetry parameter A_C at the Co $2p$ edge deduced from reflectance spectra as shown in Fig. 4, top (filled circles) and deduced from 50-nm Co film in transmission (open triangles). Inset: Graphene exhibits ferromagnetism, induced by Co, proven here by the detection of element selective hysteresis curves measured by T-MOKE at the C 1s (open squares) and Co $2p$ edge (filled circles).

is plotted in Fig. 4, bottom panel (filled symbols), reaching large values of $A_C = 0.7$ at the Co $2p_{3/2}$ resonance energy. For a quantitative evaluation additional XMCD experiments on a transmission sample at the Co $2p_{3/2}$ edge of 50-nm Co on 100-nm Si$_3$N$_4$ were performed showing $A_C(\mathrm{Co}) = 0.78$ (Fig. 4 bottom panel, open symbols). The XMCD data deduced from transmission spectra are proportional to the magnetic moment μ and the respective matrix elements [12]. From the ratio of the asymmetry parameter $A_C(C)/A_C(\mathrm{Co})$ and the magnetic moment of Co ($\mu_{Co} = 1.76\mu_B$) we obtain the magnetic moment of carbon $\mu_C = 0.14 \pm 0.03\mu_B$. An identical value is estimated when calculating the ratio of the respective integrals of the XMCD spectra across the C 1s and the Co $2p$ edges, respectively [12]. Moreover, this value of magnetic moment is confirmed independently by our T-MOKE spectra taken at the C 1s [Fig. 3(d)] and at the Co $2p$ edge (not

shown). Our μ_C is somewhat larger than recent predictions for H adsorbed on graphene [6] and a factor of 3 larger than the value obtained for a polycrystalline C layer in a Fe/C multilayer [27]. This is surprising in view of the larger magnetic moment of Fe compared to that of Co inducing the magnetism in graphene. We explain this larger magnetic moment of graphene due to the strongly aligned $\pi*$ orbitals in graphene in contrast to the random distribution of $\pi*$ orbitals in the polycrystalline carbon in Fe/C multilayers [27]. We emphasize that magnetic moments deduced in this paper as well as in Refs. [8,25,26] at the C 1*s* edge are estimations since sum rules as used for XMCD spectroscopy of the $2p - 3d$ transitions do not exist for $1s - 2p$ transitions.

E. Hysteresis curve

For a further element-selective investigation of magnetism in graphene the T-MOKE was exploited. Two element-specific hysteresis loops were recorded by setting the photon energy first to the Co $2p_{3/2}$–$3d$ transition at 775.75 eV and then to the C 1*s* resonance energy (286.3 eV) and detecting the reflected intensity as a function of the applied magnetic field strength (Fig. 4, bottom, inset). This provides the first hysteresis loop showing the individual magnetic behavior of carbon atoms in graphene, something that is not possible by classical transport experiments in the terahertz region [11]. The close relation of both hysteresis loops shows that Co induces the ferromagnetism in graphene and, moreover, graphene seems to be magnetically harder than Co. The results presented here may be further extended by comparing different azimuthal orientations of the graphene sheet for the same angle of incidence, which might shed light on the question of whether magnetic easy and hard directions are present.

F. Magneto-optical constants

The combined Faraday and XMCD experiments allowed for the determination of the magneto-optical constants of graphene. The magnetic contribution $\Delta\delta$ to the optical constant [Eq. (1)] was deduced directly from the Faraday rotation [Fig. 3(b)] according to Eq. (3a) and is plotted in Fig. 5(d). The peak value $\Delta\delta = 3.5 \times 10^{-3}$ is a factor of 3.3 larger than the value at the $2p$ edge of Co [14]. The optical constant $\Delta\beta$ [Fig. 5(b)] was deduced directly from the XMCD spectrum [Fig. 3(c)] via Eq. (3b). The peak value $\Delta\beta = 11 \times 10^{-3}$ is six times larger than the value obtained at the Co $2p$ edge [14]. To estimate the relation of these magnetic parts to the nonmagnetic parts of the optical constants independently measured spectra of nonmagnetic quasi-free-standing graphene on Cu yield are plotted in Figs. 5(a) and 5(c). These data are deduced from our near edge x-ray absorption fine structure (NEXAFS) experiments and published in Ref. [23]. With these, the relative asymmetry ratios $\Delta\delta/\delta_0$ and $\Delta\beta/\beta_0$ are in the range of 10–35%, which is similar to those observed at the Co $2p$ edge. This shows that the magnetism in graphene is strongly related to the magnetic Co substrate.

G. Alignment of $\pi*$ orbitals

The degree of alignment of $\pi*$ orbitals as well as their hybridization with Co $3d$ orbitals can be deduced qualitatively
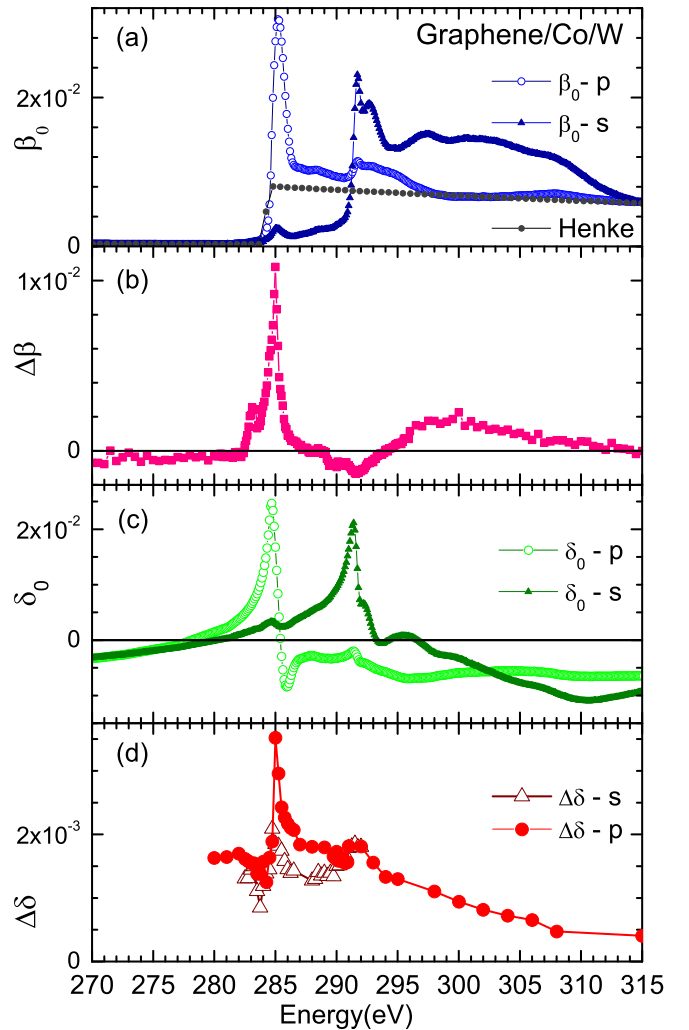

FIG. 5. Measured magneto-optical refractive indices of graphene. (a) Nonmagnetic contribution β_0 for linearly polarized light in *s* and *p* geometry, deduced from graphene on Cu via electron yield spectroscopy published in Ref. [23] and comparison with standard data taken from Henke *et al.* [19]. (b) Magnetic contribution to the absorption part $\Delta\beta$ deduced from XMCD spectra [Fig. 3(c)] via Eq. (3b) showing strongest magnetic signals at the π resonance near 285 eV. (c) Nonmagnetic contribution of the refractive part δ deduced from the absorption part [Fig. 5(a)] via Kramers-Kronig transformation [23]. (d) Magnetic contribution $\Delta\delta$ of the refractive part deduced from the Faraday rotation data [Fig. 3(b)] via Eq. (3a) showing strongest magnetic signals for *p*-polarized light at the π resonance.

from the polarization dependence of the Faraday rotation using *p*- and *s*-polarized light according to the following considerations (Fig. 6). In the ideal case of perfectly oriented graphene on Co (0001) the carbon atoms of sublattice *A* are placed on top of Co atoms while carbon atoms of sublattice *B* are above the substrate hollow sites (Fig. 6). Thus carbon atoms of sublattice *A* are expected to align their p_z orbitals perpendicularly to the graphene layer due to direct hybridization with the Co $3d_{z^2}$ orbitals (Fig. 6). As a consequence, for sublattice *A* the Faraday rotation φ_p should appear for *p*-polarized light only and vanish for *s*-polarized light. Contrary to this assumption we
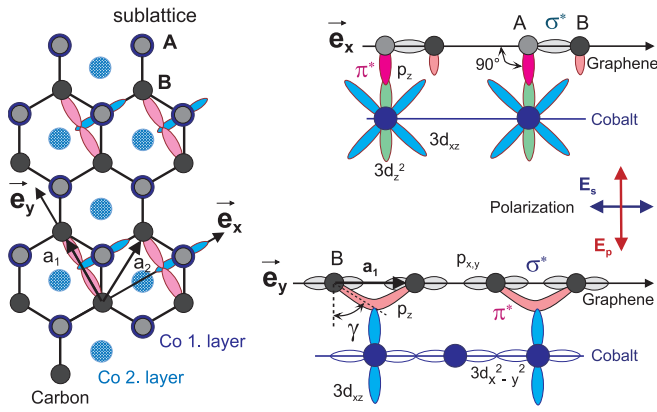
FIG. 6. Illustration of two different hybridization processes of C p_z orbitals with Co $3d$ orbitals and resulting A-B-sublattice symmetry breaking. Carbon atoms of sublattice A (gray) above Co atoms (blue) hybridize with Co $3d_{z^2}$ orbitals (green) showing perpendicular alignment (right top). Carbon atoms of sublattice B (black) above a hollow site of the Co lattice hybridize with each other (pink) and with Co $3d_{xz}$ (blue, right bottom) forming tilted p_z orbitals, which is deduced from the polarization dependence, applying E_p or E_s (right center).

observe Faraday rotation angles φ_s even for s-polarized light [Fig. 3(b), open symbols], which indicates tilted π^* orbitals with component parallel to the light's electric-field vector. This is explained by the tilt of p_z orbitals of carbon atoms of sublattice B due to hybridization with each other and with the Co $3d_{zx}$ and $3d_{zy}$ orbitals (Fig. 6). Additionally to the contribution of tilted π bondings of sublattice B a rotation of graphene flakes (see discussion of Fig. 2) and a misalignment of the graphene lattice with respect to the Co substrate lead to a reduced number of sublattice A atoms which are placed directly on top of Co atoms and an increase of carbon atoms above the substrate's hollow sites.

The remaining Co $3d_{x^2-y^2}$ and $3d_{xy}$ orbitals which are aligned in plane and directed towards the neighboring Co atoms without hybridization with carbon orbitals are expected not to contribute to the magnetization of graphene. Similarly, the carbon p_x and p_y orbitals are forming in-plane σ bonds without hybridization with Co $3d$ orbitals and thus are expected, too, to show no magnetism in our spectra.

The fact that the Faraday rotation of p-polarized light exceeds that of s-polarized light at the π^* resonance [Fig. 3(b)] indicates a predominantly perpendicular alignment of p_z-$3d$ hybridization. This finding is in agreement with observations [25,26] which show that an out-of-plane magnetization of Co can be maintained even for 20 monolayer thick Co due to coverage with graphene.

For a further discussion of different hybridizations of the A- and B-sublattice carbon atoms, respectively, and to identify the transitions at the π resonance and their assignment to A sites and B sites, total electron yield (TEY) absorption spectra for s- and p-polarized light are plotted in Fig. 7 (top, open symbols). The experimental data have been fitted (Fig. 7, top, lines) using a constant background and Lorentzians at E_1 (284.70 eV), E_2, (285.14 eV), E_3 (285.48 eV), and E_{3b} (285.95 eV). Data and fits are shown in Fig. 7, top, for the TEY
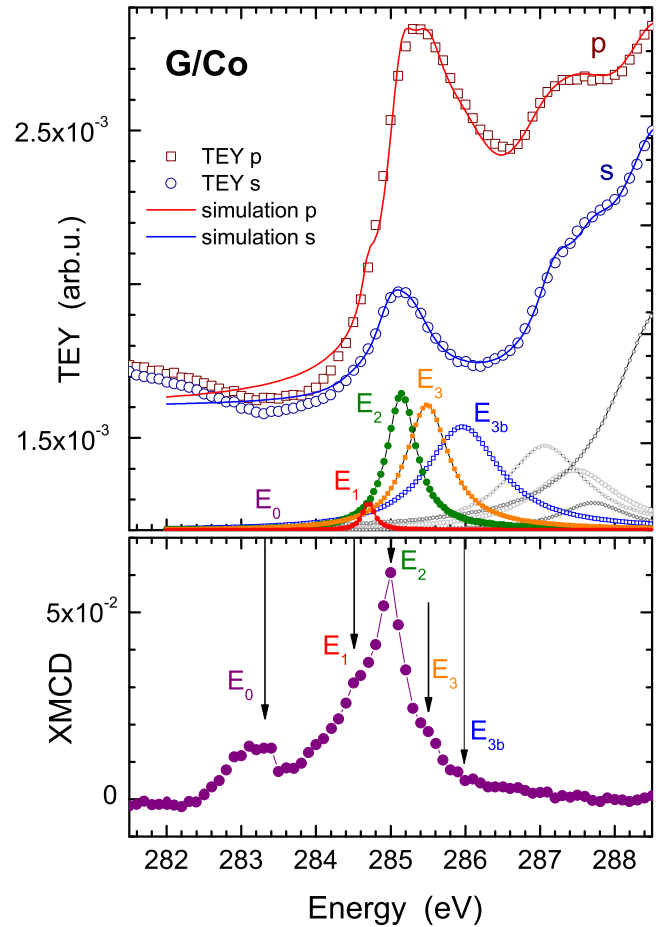

FIG. 7. Top: Total electron yield spectra for p and s polarizations (symbols) and simulations (lines) using Lorentzians at the respective transition energies, shown for p polarization. Bottom: XMCD spectrum deduced from reflection spectra with circularly polarized light and opposite in-plane magnetizations. The arrows indicate the corresponding transitions.

spectrum obtained with p-polarized light. For s-polarized light the Lorentzians are shifted by 0.2 eV to lower energies. The respective intensity ratios are $E_1(p)/E_1(s) = 7$, $E_2(p)/E_2(s) = 3$, $E_3(p)/E_3(s) = 3$, and $E_{3b}(p)/E_{3b}(s) = 27$. At energies above 287 eV shoulders have been assigned to transitions related to nonoriented adsorbates (see, e.g., Ref. [28]), which do not show polarization-dependent intensities, as can be expected. All the peaks from E_1 to E_{3b} can be excited by p- as well as by s-polarized light. Thus a strict distinction between A-site and B-site carbon atoms cannot be achieved. However, the peaks at E_1 and E_{3b}, showing the strongest p excitation may be assigned to A sites.

A comparison with the XMCD reflection spectrum in Fig. 7 (bottom) allows for an assignment of magnetic structures to the transitions associated with E_1 to E_3. Additionally, on the low-energy side the XMCD spectrum shows a structure E_0 (283.3 eV) which is hardly observable in the TEY spectra and therefore transition E_0 it is not simulated in the TEY spectra. On the high-energy side a weak XMCD shoulder may be assigned to the E_{3b} structure. Note that TEY absorption spectra represent the density of states, whereas XMCD spectra

show differences in the spin-split density of states. This may explain the observed energy shift of about 0.2 eV of the XMCD spectrum and the weak intensity of E_0 in TEY spectra. According to theory [9] we assign the first XMCD structure E_0 to lowest CB states related to A sites and E_1 related to an A-B-mixture. The next structures are assigned to higher CB states with E_3 related to A sites and E_2 related to a mixture of A- and B-site types. This is confirmed by our T-MOKE which probes perpendicularly oriented bonds at the A site resulting in strong spectral structures at E_2 and E_3 [Fig. 3(d)]. Excitations related to B sites show stronger structures for s-polarized light which also is found in our Faraday spectra [Fig. 3(b)]. Also, the strongest magnetic effects appear at E_2 and E_3 due to the strong hybridization of Co $3d_{z^2}$ with C p_z at A sites. A clear A-B splitting of CB states cannot be deduced. According to the calculations of Ref. [9] in the lower conduction band a A-B site splitting of E_1-$E_0 = 1.4$ eV and in the higher conduction band a splitting E_{3b}-$E_2 = 0.8$ eV might be deduced with a broad range of mixed A- and B-site character.

We emphasize that our interpretation is tentative. Previously, for graphene on nickel [8] a larger $A - B$ splitting of 2 eV was observed. This is possible due to the different substrates, fcc Ni (111) (Ref. [8]) versus hcp Co (0001) as investigated here. The positioning of the carbon sublattice atoms (e.g., on top of a $3d$ atom, or above a hollow site) depends on the underlying crystal structure of the substrate which will affect the bonding properties of the carbon A and B sites, which in turn leads to differences in the spectra. The $3d$ states in Co and Ni can also result in different x-ray spectra due to the different fillings of the d states with Co having $3d^7$ and Ni $3d^8$, respectively, as well as a different exchange splitting. The bonding of the carbon p orbitals to Co $3d$ orbitals can therefore differ from that of the Ni $3d$ orbitals.

Also a clear difference is found for the binding energy of the carbon $1s$ states for graphene on Ni with $E_b = 284.8$ eV [8] and for graphene on Co with $E_b = 285.3$ eV [10]. Also, the band structure differs for graphene on Ni and Co showing shifts in the band energy [3]. Thus, the experimental findings presented in our paper for graphene on Co are not inconsistent with those of Weser *et al.* for graphene on Ni [8]. STM spectroscopy and electronic band calculations presented by Eom *et al.* appear to be consistent with the interpretation given here [29].

Independently of the A-B character, the XMCD and Faraday spectra reveal that the hybridization of carbon with Co $3d$ orbitals and induced magnetism is not restricted to the Dirac point but extends over a wide range in the Brillouin zone. A similar finding was obtained by photoelectron spectroscopy for the occupied valence band [3,9,26,30].

IV. CONCLUSIONS

We have observed a giant x-ray Faraday effect at the C $1s$ edge of graphene on Co. This large magneto-optical effect results from the hybridization of Co $3d$ with carbon π^* orbitals showing different bond angles for carbon on sublattices A and B. Our findings pinpoint that to observe large x-ray magneto-optical effects a spin-orbit splitting of initial states, as is typical for $3p$ and $2p$ core levels in $3d$ transition metals, is not a prerequisite. Rather, the sublattice symmetry breaking leads to a splitting of spin-polarized final states that results in unexpectedly large magneto-optical effects. We estimated experimentally an induced magnetic moment of $0.14 \mu_B$ on carbon. Our investigations show that magneto-x-ray Faraday spectroscopy employing linearly polarized synchrotron radiation offers new access to element and bond-sensitive magnetic investigation of graphene on nontransparent metallic substrates for spintronics since it overcomes the limitations of classical transport experiments in the terahertz region that exploit the cyclotron resonance of CB electrons.

[1] A. K. Geim and K. S. Novoselov, Nature Mater. **6**, 183 (2007).

[2] K. S. Novoselov, V. I. Falko, L. Colombo, P. R. Gellert, M. G. Schwab, and K. Kim, Nature (London) **490**, 192 (2012).

[3] A. Varykhalov, D. Marchenko, J. Sánchez-Barriga, M. R. Scholz, B. Verberck, B. Trauzettel, T. O. Wehling, C. Carbone, and O. Rader, Phys. Rev. X **2**, 041017 (2012).

[4] P. Esquinazi, D. Spemann, R. Höhne, A. Setzer, K.-H. Han, and T. Butz, Phys. Rev. Lett. **91**, 227201 (2003).

[5] J. Cervenka, M. I. Katsnelson, and C. F. J. Flipse, Nat. Phys. **5**, 840 (2009).

[6] H. González-Herrero, J. M. Gómez-Rodríguez, P. Mallet, M. Moaied, and J. J. Palacios, Science **352**, 437 (2016).

[7] M. Garnica, D. Stradi, S. Barja, F. Calleja, C. Díaz, M. Alcamí, N. Martín, A. L. Vázquez de Parga, F. Martín, and R. Miranda, Nat. Phys. **9**, 368 (2013).

[8] M. Weser, Y. Rehder, K. Horn, M. Sicot, M. Fonin, A. B. Preobrajenski, E. N. Voloshina, E. Goering, and Yu. S. Dedkov, Appl. Phys. Lett. **96**, 012504 (2010).

[9] D. Marchenko, A. Varykhalov, J. Sánchez-Barriga, O. Rader, C. Carbone, and G. Bihlmayer, Phys. Rev. B **91**, 235431 (2015).

[10] D. Marchenko, A. Varykhalov, M. R. Scholz, G. Bihlmayer, E. I. Rashba, A. Rybkin, A. M. Shikin, and O. Rader, Nat. Com. **3**, 1232 (2012).

[11] I. Crassee, J. Levallios, A. L. Walter, M. Ostler, A. Bostwick, E. Rotenberg, T. Seyller, D. v.d. Marel, and A. Kuzmenko, Nat. Phys. **7**, 48 (2011).

[12] J. Stöhr and H.C. Siegmann, *Magnetism: From Fundamentals to Nanoscale Dynamics* (Springer, Berlin, 2006).

[13] F. Schäfers, H.-Ch. Mertins, A. Gaupp, W. Gudat, M. Mertin, I. Packe, F. Schmolla, S. Di Fonzo, G. Soullié, W. Jark, R. Walker, X. Le Cann, M. Eriksson, and R. Nyholm, Appl. Opt. **38**, 4074 (1999).

[14] H.-Ch. Mertins, F. Schäfers, X. Le Cann, A. Gaupp, and W. Gudat, Phys. Rev. B **61**, R874 (2000).

[15] H.-Ch. Mertins, P. M. Oppeneer, J. Kunes, A. Gaupp, D. Abramsohn, and F. Schäfers, Phys. Rev. Lett. **87**, 047401 (2001).

[16] P. M. Oppeneer, in *Handbook of Magnetic Materials*, edited by K. H. J. Buschow (Elsevier, Amsterdam, 2001), Vol. 13, pp. 229–422.

[17] C. Jansing, H.-Ch. Mertins, M. Gilbert, H. Wahab, H. Timmers, S.-H. Choi, A. Gaupp, M. Krivenkov, A. Varykhalov, O. Rader, D. Legut, and P. M. Oppeneer, Phys. Rev. B **94**, 045422 (2016).

[18] F. Schäfers and M. Krumrey, REFLEC, BESSY Technical Report No. TB 201,1996 (unpublished).

[19] B. L. Henke *et al.*, http://www-cxro.lbl.gov/optical_constants/asf.html.

[20] M. R. Weiss, R. Follath, K. J. S. Sahawney, F. Senf, J. Bahrdt, W. Frentrup, A. Gaupp, S. Sasaki, M. Scheer, H.-Ch. Mertins, D. Abramsohn, F. Schäfers, W. Kuch, and W. Mahler, Nucl. Instrum. Meth. A **467–468**, 449 (2001).

[21] C. Jansing, H.-Ch. Mertins, A. Gaupp, A. Sokolov, M. Gilbert, H. Wahab, and H. Timmers, J. Phys.: Conf. Series **712**, 012031 (2016).

[22] M. F. Tesch, D. Legut, H.-Ch. Mertins, M. C. Gilbert, C. Jansing, J. Hamrle, J. Rusz, P. M. Oppeneer, D. E. Bürgler, C. M. Schneider, A. Gaupp, and U. Berges, Phys. Rev. B **89**, 140404(R) (2014).

[23] H. Wahab, C. Jansing, H.-Ch. Mertins, J. H. Kim, S.-H. Choi, A. Gaupp, and H. Timmers, Carbon **137**, 252 (2018).

[24] H.-Ch. Mertins, D. Abramsohn, A. Gaupp, F. Schäfers, W. Gudat, O. Zaharko, H. Grimmer, and P. M. Oppeneer, Phys. Rev. B **66**, 184404 (2002).

[25] H. Vita, S. Böttcher, P. Leicht, K. Horn, A. B. Shick, and F. Maca, Phys. Rev. B **90**, 165432 (2014).

[26] H. Vita, S. Böttcher, K. Horn, E. N. Voloshina, R. E. Ovcharenko, Th. Kampen, A. Tissen, and Yu. S. Dedkov, Sci. Rep. **4**, 5704 (2014).

[27] H.-Ch. Mertins, F. Schäfers, and A. Gaupp, Europhys. Lett. **55**, 125 (2001).

[28] A. Gaupp, F. Schäfers, M. MacDonald, S. Uschakow, N. N. Slashchenko, and P. K. Gaykovich, J. Phys.: Conf. Series **425**, 122013 (2013).

[29] D. Eom, D. Prezzi, K. T. Rim, H. Zhou, M. Lefenfeld, S. Xiao, C. Nuckolls, M. S. Hybertsen, T. F. Heinz, and G. W. Flynn, Nano Lett. **9**, 2844 (2009).

[30] A. D. Vu, J. Coraux, G. Chen, A. T. N'Diaye, A. K. Schmid, and N. Rougemaille, Sci. Rep. **6**, 24783 (2015).